MSDE

PAPER

View Article Online
View Journal | View Issue

Check for updates

Cite this: *Mol. Syst. Des. Eng.*, 2024, **9**, 518

Corrosion inhibitor screening for AA6014 aluminum alloy under different ambient conditions using a novel multielectrode methodology

Chathumini Samarawickrama, *[a] Sebastian Pöhlker,[b] Paul White, [a] Ivan Cole *[a] and Patrick Keil *[ab]

Received 15th January 2024,
Accepted 23rd February 2024

DOI: 10.1039/d4me00013g

rsc.li/molecular-engineering

Atmospheric corrosion, an electrochemical phenomenon, initiates the degradation of materials, primarily metals, through their interaction with environmental droplets or aerosols. This degradation extends to various aspects such as material performance, longevity, and safety, emphasizing the critical need to comprehend and inhibit corrosion, particularly in industrial and environmental settings. Structural aluminum alloys, prominently used in aerospace, automotive, and marine industries, undergo extensive scrutiny due to their susceptibility to atmospheric corrosion. Nonetheless, the absence of suitable electrochemical techniques capable of accommodating droplet volumes underscores the urgent need for advancements in corrosion research. This paper introduces an innovative and efficient multielectrode cell setup aimed at rapid screening of droplet and thin film electrolyte volumes, presenting a new high-throughput screening method. Utilizing AA6014 as a substrate, this paper demonstrates a proof of concept for this methodology. It explores the influence of a crucial parameter, pH, while considering the effects of evaporation and secondary spreading. Various organic corrosion inhibitors, including some well-known inhibitors, were examined to evaluate the impact of chemically related structures on inhibition efficiency. This investigation predominately focuses on comparing and discussing differences and similarities in inhibition performance between bulk and droplet volumes. Ultimately, this comprehensive investigation aims to enhance the understanding and management of corrosion inhibition in droplet and thin film environments.

Design, System, Application

Our investigation delves into the comprehension and management of corrosion inhibition in different electrolyte geometries, focusing on enhancing the understanding of the differences in corrosion mechanisms between bulk volumes and droplet/thin-film electrolytes. Our study introduces an innovative electrochemical cell setup that rapidly screens corrosion inhibitors in droplet volumes, providing a more realistic representation of atmospheric corrosion scenarios and a more accurate understanding of inhibitor effectiveness. This approach enables a precise evaluation under droplets, aiding in the thoughtful selection of corrosion inhibitors for applications involving corrosion under droplets, like in atmospheric corrosion or cabinet corrosion testing. In addition, our study aims to enhance the design of chemical structures by providing a better understanding of the role of diverse chemical structures on corrosion inhibition in real conditions. A proper choice of corrosion inhibitors can minimise maintenance costs, ensuring enhanced durability and longevity of materials in corrosive environments. The use of effective protective methods against corrosion contributes to sustainable practices by minimizing metal production, marking a positive step towards environmental responsibility. Overall, this comprehensive investigation provides valuable insights into corrosion inhibition in droplet and thin film environments, enabling informed decisions for sustainable and cost-effective material protection.

1. Introduction

Corrosion is an electrochemical process that leads to the degradation and deterioration of materials, primarily metals, by their interaction with the environment. The consequences of corrosion are far-reaching and can have a significant impact on the performance, longevity, and safety of materials, structures, and equipment. The study of corrosion under droplets and its inhibition is of immense importance due to its relevance in various industrial and environmental applications. Corrosion under droplets occurs when a small amount of liquid, usually water, encounters a metal surface.

[a] *RMIT University, Melbourne, VIC 3001, Australia. E-mail: chathumini.sama@gmail.com, ivan.cole@rmit.edu.au*
[b] *BASF Coatings GmbH, Glasuritstrasse 1, 48165 Muenster, Germany. E-mail: patrick.keil@basf.com*

The presence of a droplet creates a localised environment that can lead to accelerated corrosion rates and the formation of corrosion products, which can ultimately lead to material failure.[1–5] This type of corrosion is especially critical in industries such as oil and gas (land-based), transportation, and utilities, where the integrity and reliability of infrastructure are paramount. A key factor in understanding and mitigating corrosion under droplets is the study of its inhibition, which is most commonly achieved through protective coatings and/or corrosion inhibitors, and in the case of active protection by coatings, leached inhibitors need to be active under droplets to provide protection.

The widespread use of aluminum alloys in the automotive and aerospace sectors has prompted a thorough investigation into their corrosion resistance.[6–9] In automotive industry, the preference often lies with 6000 series alloys such as 6014, 6016, 6022 and 6111 due to their remarkable corrosion resistance, weldability, and cost-effectiveness.[10,11] The other 6000 series alloys such as 6060 and 6061 are more often used in the construction industry. Moreover, their versatility extends to manufacturing processes, as they can be easily extruded to form sections with intricate geometries. The strength of 6000 series alloys can be enhanced through heat treatment, ensuring that they meet the stringent performance requirements expected in automotive and construction applications while maintaining their structural integrity under challenging conditions.[10] In recent years, the exploration of organic and inorganic multifunctional inhibitors has been motivated by the desire to minimise costs and risks associated with corrosion. However, much of the existing research in this area has focused on using a bulk volume of electrolyte for immersion or electrochemical testing.[6,12] It is important to note that atmospheric corrosion is a complex process influenced by various factors, including moisture condensation in the atmosphere due to temperature changes and the hygroscopic effects of surface contaminants, leading to droplet formation on surfaces.[1,2,13–17]

The rate of atmospheric corrosion is significantly impacted by the characteristics of these droplets, including their size and population densities, which are determined by atmospheric humidity, temperature, surface temperature, and wettability.[15,17–27] Previous studies have highlighted the differences in corrosion mechanisms between droplet environments and conventional bulk volume electrolytes. In bulk electrolytes, oxygen diffusion through the electrolyte can control the corrosion rate and be measured as a diffusion-limited current. With a reduced droplet volume, oxygen can more effortlessly diffuse through a much shorter path from the atmosphere to the metal surface.[16,28,29] This increased accessibility of oxygen accelerates the occurrence of corrosion reactions.

Many studies have focused on using bulk volume electrolytes, but limited research has been published regarding corrosion in connection with droplet or thin-film electrolytes.[14–17,21,24,27,30,31] There is a scarcity of information about the effectiveness of corrosion inhibitors in preventing corrosion under droplet conditions.

In recent times, the adoption of multielectrode cells has gained popularity as an effective method for rapid screening of corrosion inhibitors.[32–35] This approach enables the attainment of steady-state conditions almost instantaneously and simultaneous determination of both anodic and cathodic inhibition, which is very important for rapid screening of multi-functional inhibitor formations. In this study, a novel multielectrode cell is introduced, designed specifically to accommodate droplet or thin-film electrolytes, enabling rapid screening of electrochemical testing.[33,34,36] This allows to comprehend how the chemical structures of the inhibitors impact their ability to inhibit corrosion in both environments and provide valuable insights for corrosion control strategies in real-world applications. The aim of this paper is to validate the proposed inhibitor screening method in droplet volumes and to explore the performance of a range of chemically related compounds both in bulk and droplet volumes to determine the effect of the chemical structures on inhibiting droplet corrosion and immersion corrosion of aluminium alloy AA6014.

2. Material and methods

2.1 Substrate preparation

The automotive-quality aluminium alloy AA6014 was supplied by Chemetall GmbH, Germany. The samples were cut into 52 mm × 20 mm × 1 mm size plates, which were then cleaned with ethanol and dried with an N_2 gun. As shown in Fig. 2, two identical cut metal samples were then embedded in an epoxy resin mould 40 mm in diameter. The exposed faces of the metal samples were abraded using 400, 1200 and 2500 grit SiC paper to a mirror finish. The sample was then rinsed with ethanol, dried using N_2 and stored in a desiccator until further use.

2.2 Electrolyte preparation

The experiment utilised compounds sourced from Sigma Aldrich, with inhibitor solutions prepared at either 1 mM or 10 mM concentration in a 5 wt% NaCl base solution. The solutions were stirred using a magnetic stirrer at room temperature until the inhibitors were fully dissolved and then aerated with compressed air to ensure oxygen saturation. The pH of the solutions was adjusted to pH 7 before testing, unless otherwise specified, using dilute NaOH or HCl as needed to achieve neutral pH conditions.

To act as controls, a previous study by Harvey *et al.* created a database of compounds, including well-known corrosion inhibitors.[12] A range of chemically related compounds that could form metal–organic surface complexes were chosen from the Harvey *et al.* dataset.[12] The selected range of chemical compounds is outlined in Table 1 below.

Fig. 1 depicts chemically related structures through the use of coloured circles, which serve to emphasize essential

Table 1 A list of selected range of chemical compounds for corrosion inhibition

Identifier	Inhibitor	Type of inhibitor
1A	4,5-Diamino-2,6-dimercaptopyrimidine	Mixed
1B	4,5-Diaminopyrimidine	Mixed
1C	Na-(Diethyl(dithiocarbamate))	Cathodic
1D	2-Mercaptopyrimidine	Mixed
1E	Pyrimidine	Mixed
1G	Na-Benzoate	Anodic
1I	Pyridine	Mixed
1J	Na-(4-Phenylbenzoate)	Anodic
1K	Na-(4-Hydroxybenzoate)	Anodic
1L	Na-(4-Mercaptobenzoate)	Anodic
1M	Na-(6-Mercaptonicotinate)	Mixed
1N	Na-Nicotinate	Mixed
1O	Na-Iso-nicotinate	Mixed
1P	Na-Picolinate	Mixed
1Q	Na-(3-Mercaptobenzoate)	Anodic
1R	Na-Salicylate	Mixed
1S	Na-(2-Mercaptobenzoate)	Anodic
1T	Na-(2-Mercaptonicotinate)	Mixed
1X	Na-Acetate	Anodic
2A	2,5-Dimercapto-1,3,4-thiadiazole	Mixed
2B	Benzotriazole	Mixed
2D	6-Amino-2-mercaptobenzothiazole	Mixed
2E	2-Mercaptobenzothiazole	Mixed

functional groups, thereby highlighting the structural interconnections among the compounds.

2.3 Electrochemical method

2.3.1 Multielectrode system. The multielectrode (ME) system, initially proposed by Taylor and Chambers,[33] was introduced to analyse multiple metals in the same solution concurrently. This approach has been widely adopted in various studies.[32,34,37] In this study, this ME technique has been applied, employing the same metal substrate.

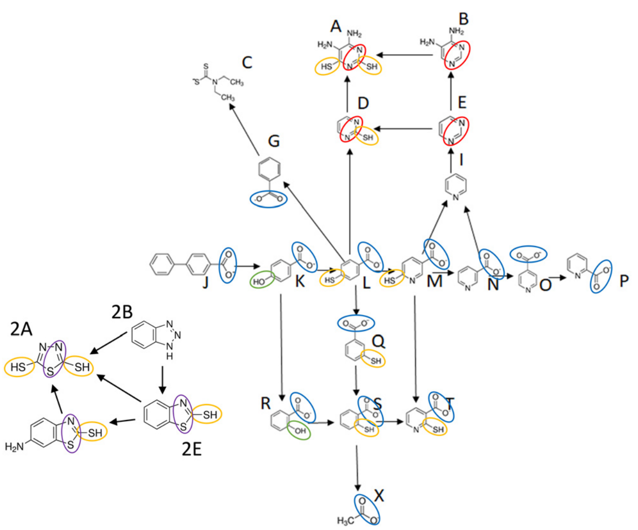

Fig. 1 Illustration of the chemical structures of inhibitors listed in Table 1 highlighting their structural relationships by using coloured circles to represent similar sub-structures.

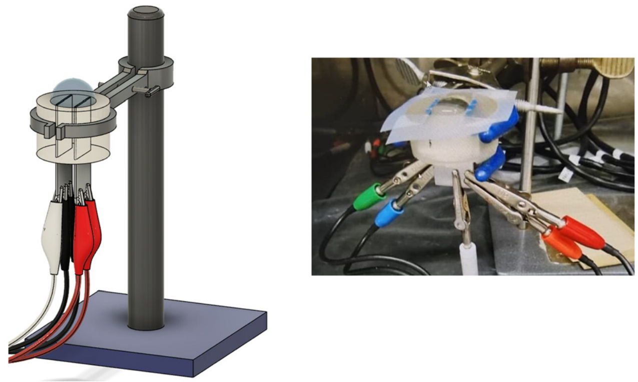

Fig. 2 An illustration of the electrochemical cell setup for droplet geometry system.

Both droplet and bulk volume testing utilized a multielectrode setup, and the electrochemical cell arrangement for droplet volume and bulk volume testing is illustrated in Fig. 2 and 3 respectively. To confine a droplet volume of 800 μL within the epoxy resin mould while exposing the metal area, scotch tape was utilized around the metal plates to delineate the boundaries, as depicted in Fig. 2.

The configuration involved connecting the reference electrode and the counter electrode and coupling them with one metal sample, while the working electrode was connected to the other metal sample, as illustrated in Fig. 2.[32]

Fig. 3 illustrates the cell arrangement designed for bulk volume testing, aiming to ensure uniform conditions and experimental methodologies. An identical epoxy mould setup as per the droplet system was employed. The mould was submersed in 80 ml of electrolyte, ensuring that the exposed metal surface came into contact with the electrolyte solution interface.

All electrochemical experiments were performed using a Gamry Reference 1000 potentiostat with a multielectrode cell setup.

In the interest of evaluating the inhibitor performance, the below test sequence was followed.[37]

1. Upon immediate exposure to the corrosive environment in the presence or absence of an inhibitor, the system was allowed to reach a steady state by monitoring the open circuit potential (OCP) for 10 min.

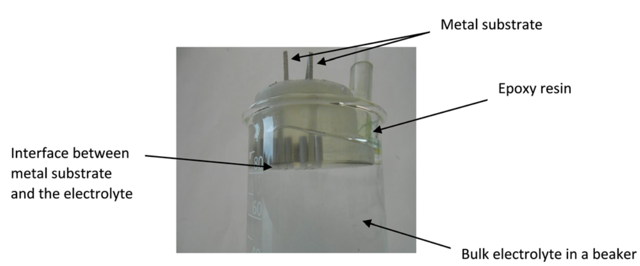

Fig. 3 The multielectrode setup for the bulk volume system utilizing the same epoxy resin cell.

2. Conduct cathodic polarization with an applied potential of −10 mV *vs.* OCP for 60 seconds.

3. The system was allowed to remain at the OCP for the next 30 seconds.

4. Conduct anodic polarization with an applied potential of +10 mV *vs.* OCP for 60 seconds.

5. The system was allowed to remain at the OCP for another 30 seconds.

6. The above-mentioned steps were repeated with gradual increments of 50 mV in potential up to ±300 mV. The current was monitored for 60 seconds of cathodic and anodic polarization.

7. The mean of the current measured over the 60 seconds for the cathodic and anodic polarization was calculated separately.

8. Then, the average of the absolute values from anodic and cathodic polarization was determined and plotted for each applied potential.

In the context of all droplet experiments, meticulous consideration should be given to the evaporation of the droplet. However, the observed evaporation rate of the 800 μL droplet during this one-hour period could be deemed inconsequential.

When employing active protection through coatings, the inhibitors must remain effective when exposed to droplets. Typically, these inhibitors become active in response to damage or abrasions on the coating, leading to their release. This safeguards the exposed metal surface and maintains the integrity of the underlying substrate. Consequently, the inhibitors must exhibit their protective properties when in a solution. This rationale underscores the importance of conducting electrochemical testing with inhibitors in solution rather than on pre-coated metal substrates, as it closely simulates real-world conditions and responses.

The proposed multielectrode system in this study facilitates the investigation of two metal samples with identical sizes and characteristics, aligning the system at 0 V and 0 A. Consequently, the time required for the system to reach a steady state is minimized, reducing the overall experimental duration. This is particularly advantageous in addressing concerns related to droplet evaporation, making shorter experimental times a distinct benefit. Moreover, this expeditious approach can prove beneficial for rapidly attaining steady states in the case of complex alloys with heterogeneous compositions, ensuring minimal alteration of the substrate surface before conducting scans.

This innovative rapid screening technique can be applied to assess a wide range of inhibitors and investigate various corrosion parameters under droplet conditions. Simple polarization tests can offer insights into the influence of electrolyte pH, droplet volume, evaporation, the evolution of droplet corrosion over time, ambient conditions such as humidity and temperature, and even the impact of sat density in the electrolyte.

A primary limitation of this multielectrode system is its restricted compatibility with various electrochemical techniques, rendering it unsuitable for applications such as linear polarization. While the setup is suitable for Electrochemical Impedance Spectroscopy (EIS), caution is advised when fitting equivalent circuits, as this process may become more complex. Additionally, in EIS experiments, achieving low frequencies requires extended durations, increasing the risk of significant droplet evaporation over time. Instead, techniques such as Odd Random Phase Electrochemical Impedance Spectroscopy (ORP-EIS) can be used to evaluate corrosion inhibitor behaviour by examining the non-linearities.[38] However, incorporating micro counter and reference electrodes with the same cell setup enables the establishment of a conventional 3-electrode system capable of accommodating droplet volumes. This adaptation provides the opportunity to employ a wide range of traditional electrochemical techniques for testing droplet volumes.

3. Results and discussion

3.1 Multielectrode system

3.1.1 Measurement system analysis (MSA). In order to assess the variation in data associated with the proposed methodology and the electrochemical setup, a measurement system analysis (MSA) was carried out. MSA is a process that evaluates the accuracy and precision of a system or test method by examining the scatter in data. Steel was chosen as the substrate for the MSA to ensure practicality, as it is more susceptible to corrosion than aluminium alloys.

The proposed cell setup was tested for both droplet and bulk volume experiments, with each configuration producing 30 independent measurements. For this series of experiments, a 5 wt% NaCl solution served as the electrolyte, and the same test sequence outlined previously was repeated, with variations introduced in the potentiostat, a batch of the electrochemical cell setup, and a batch of the electrolyte (Fig. 4).

The MSA was conducted for steel with electrophoretic deposition (ED) coated steel. The ED-coated samples exhibited 10% variation in bulk volume measurements and approximately 20% variation in droplet volume measurements. As the variation percentage remained below 20%, this technique proved to be a viable method for testing droplet volumes, with potential for

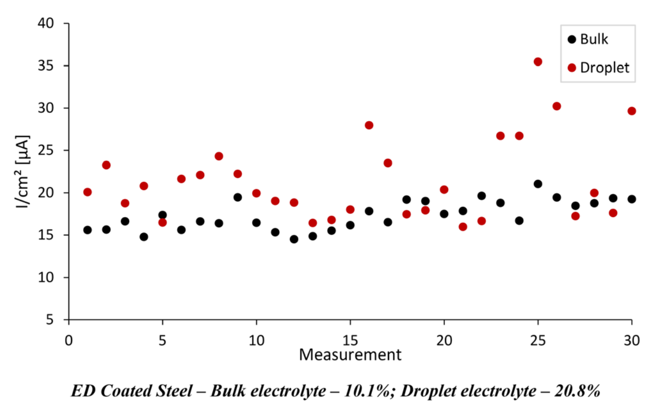

Fig. 4 The current recorded for 30 different measurements with the ME setup.

further improvements. The ED coating played a role in minimizing the potential for crevice corrosion, which is an essential consideration in testing. Moreover, the volume measurements, accurate down to 0.1 microliter, suggest that the variation attributable to the measured volume may be insignificant. Nevertheless, it is important to note that while the droplet volume remains constant, the droplet curvature might exhibit variations during measurements, depending on how the droplet is pipetted. This variability in droplet curvature and the contact angle or droplet geometry can significantly impact the corrosion current by influencing the oxygen diffusion path. As a result, careful consideration of droplet geometry becomes crucial when interpreting corrosion data in such experiments.[13,17,39] Additional factors contributing to the high scatter in data include droplet spreading and evaporation. These processes not only influence the oxygen transportation path but also increase the salt and inhibitor concentration, resulting in variations in the corrosion current, which could be observed as noise. Despite these inherent variations, the proposed methodology remains valuable for the rapid screening of inhibitors, facilitating the evaluation of both effective and ineffective inhibitors.

3.1.2 Polarization test. A preliminary set of experiments was carried out to investigate the effect of applied potential on corrosion current by varying the polarization magnitude. The testing protocol outlined in section 2 was utilized for both bulk electrolyte and droplet geometries, with and without an inhibitor. In this series of experiments, a solution comprising 1 mM pyrimidine in 5 wt% NaCl was employed as the base solution on an AA6014 metal substrate.

The graph below displays data from three replicates, aiming to evaluate the impact of applied potential on current. The current data depicted in the graph represents the average values recorded during both cathodic and anodic polarization, achieved by applying positive and negative potentials to the ME system (Fig. 5).

Similar trends are observed in both bulk and droplet volumes for inhibited and uninhibited scenarios. In the droplet geometry, the current steadily increases, while in the bulk electrolyte system, it plateaus after reaching approximately 250 mV for both inhibited and uninhibited systems. The difference in current between inhibited and uninhibited systems is smaller at low polarization levels compared to high polarization values.

Significantly, the inhibited droplet system shows less variation between repeats than the bulk volume system, as indicated by the error bars accompanying each data point. However, the uninhibited systems exhibit notable variations in the low and mid ranges of applied potentials in both bulk and droplet volumes.

The variation among repetitions is notably less for the bulk system without an inhibitor than for the droplet without an inhibitor. This difference may be attributed to more pronounced changes in the droplet solution, leading to more significant fluctuations in electrolyte composition and conditions during electrochemical reactions. Additionally, in a droplet or thin-layer geometries, the non-uniform thickness influences the oxygen concentration profile, accelerating the cathodic process at the droplet edge and acting as an anode in the centre. These variations in thickness affect the oxygen diffusion path to the metal surface, influencing the corrosion rate.[15]

3.2 Effect of pH

In droplet corrosion, electrochemical measurements are conducted using a mere 800 μL of electrolyte. The significance of such a small electrolyte volume lies in the heightened

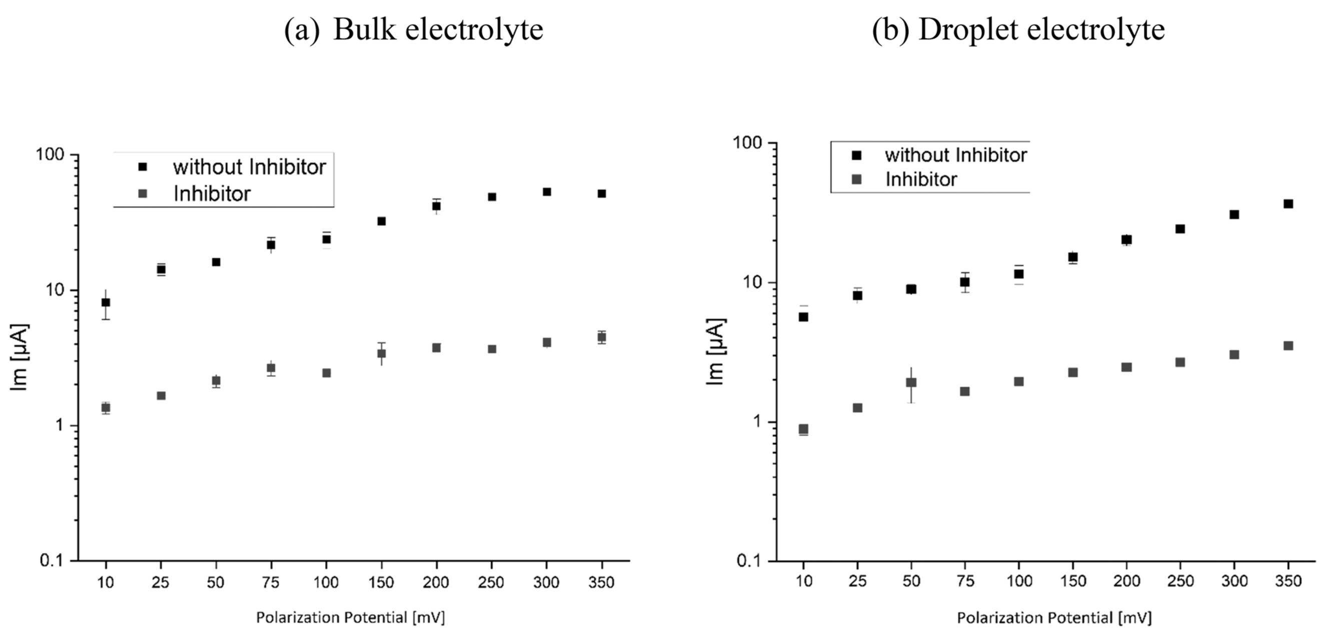

Fig. 5 The polarization test results for (a) bulk volume system (b) droplet volume system.

sensitivity to alterations in pH resulting from the metal's corrosion, potentially exerting a substantial impact on the corrosion process. Consequently, it becomes imperative to comprehend how the efficiency of inhibitors may vary depending on the solution's pH.

For this study, pH values of 3, 7, and 12 have been selected based on their potential effects on corrosion. It is plausible that inhibitors may not undergo a complete reaction with the electrodes due to the brief test duration. Simultaneously, the effectiveness of these inhibitors could be influenced by the passive range of aluminium oxide, typically falling within pH values ranging from approximately 4 to 9, according to the Pourbaix diagram, with variations based on temperature.[32,40] Metal dissolution tends to make the surrounding electrolyte acidic, and choosing a pH less than 3 may induce pitting corrosion.[41] Conversely, a pH of 12 is preferred due to the possibility of cathodic delamination in coatings, resulting in an alkaline electrolyte ranging between 12 and 14. Testing cathodic inhibitors under these conditions is essential to explore their performance.

Generally, corrosion is expected to be accelerated at very low and high pH levels. Hence, the majority of inhibitors are anticipated to exhibit better performance at a more neutral pH. For the alloy AA6014, it has been reported that Mg_2Si acts as an anode due to the anodic corrosion potential of the Al matrix.[6,42] Consequently, these intermetallic particles preferentially dissolve concerning the Al matrix in neutral and acidic conditions.

Fig. 6 presents the results collected for all inhibitors at a concentration of 10 mM. It compares their inhibition efficiency percentages in both bulk volume and droplet electrolytes at initial electrolyte pH values of 3, 7, and 12. The graphs illustrate the inhibition efficiency percentage with bulk volume on the *x*-axis against the inhibition efficiency percentage with droplet volume on the *y*-axis.

The inhibition efficiency (IE%) was computed using the following equation.

$$\text{IE\%} = \left[1 - \frac{i_{\text{corr}}\ (\text{with inhibitor})}{i_{\text{corr}}\ (\text{without inhibitor})}\right] \times 100$$

These graphs are categorized into four quadrants, aiding in understanding inhibitor performance in bulk and/or droplet volumes:

1. Only performs well in droplet volume.
2. Performs well in both bulk and droplet volume.
3. Performs poorly in both bulk and droplet volume.
4. Only performs well in bulk volume.

This analysis assists to understand the performance of inhibitors in bulk and/or droplet volumes.

For AA6014 at pH 7, most inhibitors show similar performance in both bulk and droplet volumes. However, at pH 3, a notable contrast emerges, with inhibitors performing relatively better in bulk volume compared to droplet volume and in general, most inhibitors perform poorly at pH 3. In fact, in droplet volumes, most inhibitors display a pronounced increase in corrosion rates.

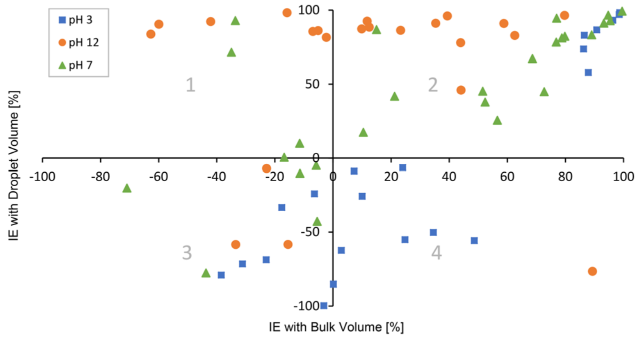

Fig. 6 Comparison between the inhibition efficiency of a range of compounds on AA6014 in bulk volume and droplet volume.

Conversely, at pH 12, over 81% of the displayed inhibitors demonstrate high levels of inhibition in droplet volume, while only about 45% of the displayed inhibitors exhibit inhibition in bulk volume. Overall, at pH 12, inhibitors perform significantly better in droplet volume, while at pH 7, their performance is only slightly superior to that in bulk volume, followed by the substantial drop at pH 3, mentioned above.

3.3 Effect of molecular structure

Analysing the presented data, it becomes evident that chemical functionalities have distinct effects on droplet and bulk volumes. Therefore, assuming that the same inhibitors would be equally effective in both applications would be inaccurate.

Based on the inhibitor's chemical structure and composition, it was possible to depict a range of effects of various chemical functionalities on corrosion behaviour.

Most pyridine derivatives demonstrated moderate inhibition in droplet volume and comparatively higher inhibition in bulk volume, as illustrated in Fig. 7 when comparing the inhibitor compounds **1I**, **1E**, and **1B**. The presence of a –SH (thiol) group notably decreased inhibition efficiency in bulk volume for alloy AA6014. Pyrimidine derivatives **1A**, **1B**, **1D**, and **1E** exhibited medium to high inhibition efficiency in all cases (**1B**, **1E**), except for **1D**, which acted as an effective inhibitor in droplet volume but functioned as a corrosion accelerator in bulk volume.

All inhibitors displayed poor to negative inhibition efficiencies at pH 12 in bulk volume and high efficiencies in droplet volume, especially those containing a thiol group (**1A** and **1D**). At pH 3, all inhibitors showed low to medium inhibition efficiency in bulk volume and demonstrated corrosion acceleration in droplet volume, except pyridine (**1E**).

As per Fig. 8, at neutral pH, the changes are only marginal for both bulk and droplet volumes. However, apart from inhibitor compound **1S**, which has both a carboxylate and a –SH group, the other compounds (**1L**, **1M**, **1Q**, and **1T**) exhibit excellent inhibition in all scenarios. The positioning of the substituents may play a significant role, as evidenced by the results with compounds **1P** and **1S**. It's clear that both of these compounds

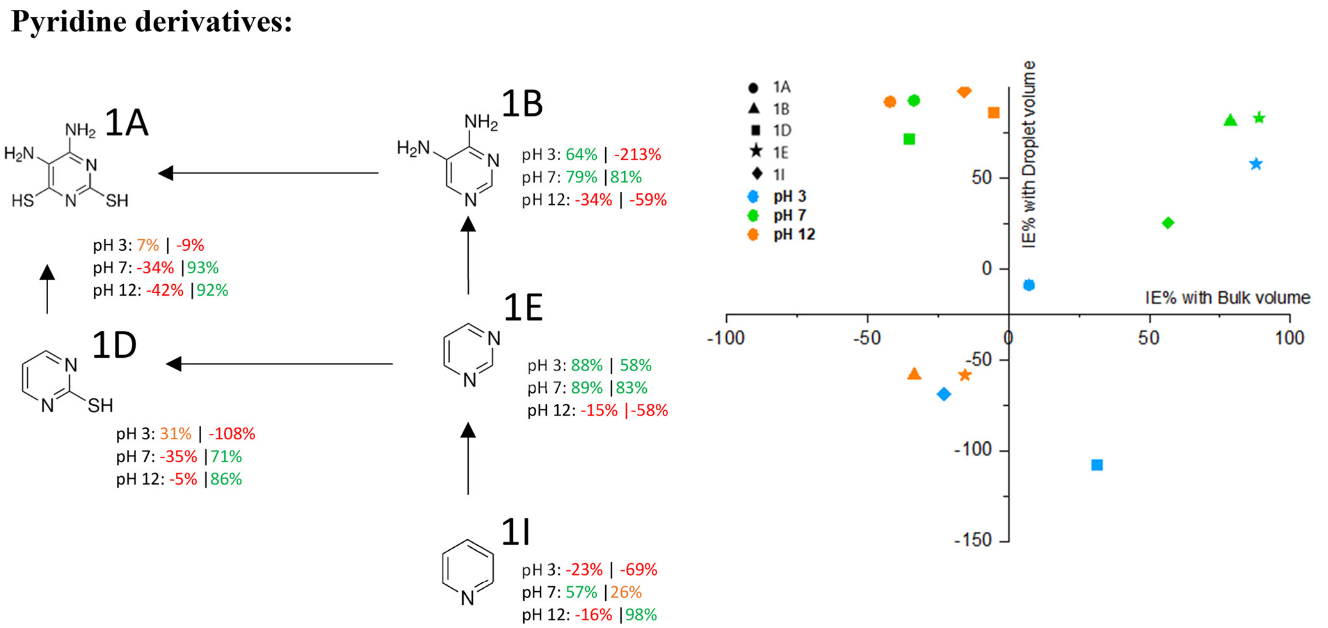

Fig. 7 The inhibition efficiency of pyridine derivatives in AA6014 (pH *x*: droplet IE%|bulk IE%).

(**1P** and **1S**) have substituents in the *ortho* position relative to the carboxylate group, and this position may not be advantageous.

In droplet volumes, the majority of inhibitors with a carboxylic group demonstrate excellent inhibition at a high pH value of 12 but act as strong corrosion accelerators at pH 3. Conversely, some inhibitors exhibit acceleration in bulk volume, while others display mediocre efficiencies at pH 3 and 12, except for inhibitors **1S** and **1T**. These two inhibitors feature a thiol group in the *ortho* position, which likely influences their exceptional performance.

Across the group of compounds, it becomes evident that the presence of a thiol group positively impacts inhibitory effects in both bulk and droplet volumes (Fig. 9). Introducing a thiol group (**1M**) to pyridine monocarboxylate (**1N**) has enhanced the performance in terms of corrosion inhibition, whether in bulk volume or droplet corrosion. Similar results are observed when substituting a thiol group from benzoate (**1G**) to 2-mercaptobenzoate (**1L**). The only exceptions are **1S** and **1D**, which might be attributed to their *ortho* positioning, as discussed previously, and the influence of nitrogens in the benzene ring, which withdraw electrons from the thiol group. Nonetheless, compound **1S** stands out with outstanding performance at pH 3 compared to other compounds featuring a thiol group. Another subtle yet notable trend is that the majority of compounds containing a thiol group exhibit a slight improvement in droplet volume compared to bulk volume. Interestingly, adding a thiol group to a pyrimidine (**1E**) seems detrimental to inhibitor performance across all conditions except for droplet volume at pH 12.

Under neutral conditions, it becomes evident that introducing a hydroxyl group promotes and accelerates corrosion in both bulk and droplet volumes, as observed in compounds **1K** and **1R**. Interestingly, the sulphur analogue exhibits significantly improved inhibitory capacity despite oxygen and sulphur being chemically related. This distinction is noticeable when comparing phenols **1K** (pH 7: −109%|−44%) and **1R** (pH 7: −105%|−70%) with thiophenols **1L** (pH 7: 93%|91%) and **1Q** (pH 7: 95%|97%) (Fig. 10).

Inhibitors containing a hydroxyl group generally perform poorly at all three pH values, except at pH 12, where inhibitor **1R** performs better in bulk, while **1K** performs better in droplet volume. This variation may be attributed to the specific position of the hydroxyl group. Substituting the hydroxyl group with a thiol group (**1R** to **1S**) results in a significant increase in inhibition efficiency across all pH values.

The introduction of an amino group seems to have a limited impact between droplet and bulk volumes at pH 7 except for compound **1A.** However, a notable contrast is observed at pH 3 and pH 12. When we compare inhibitors **1A, 1B**, and **2D** at pH 3 with their base compounds, there is a significant decrease in performance in bulk and droplet volumes. While incorporating a thiol group into compound **1B** enhanced inhibition in droplet volume, the opposite effect was observed in bulk volume (Fig. 11).

3.4 Overall discussion

The compound database, previously investigated by Harvey *et al.*,[12] covers neutral compounds and sodium salts. This study not only assesses inhibitor performance in droplet volumes but also explores the impact of pH on inhibitor effectiveness.

In bulk electrolyte corrosion, the primary factor is the rate of oxygen diffusion through the electrolyte. In the case of aluminium alloy 6014, the primary intermetallic inclusions

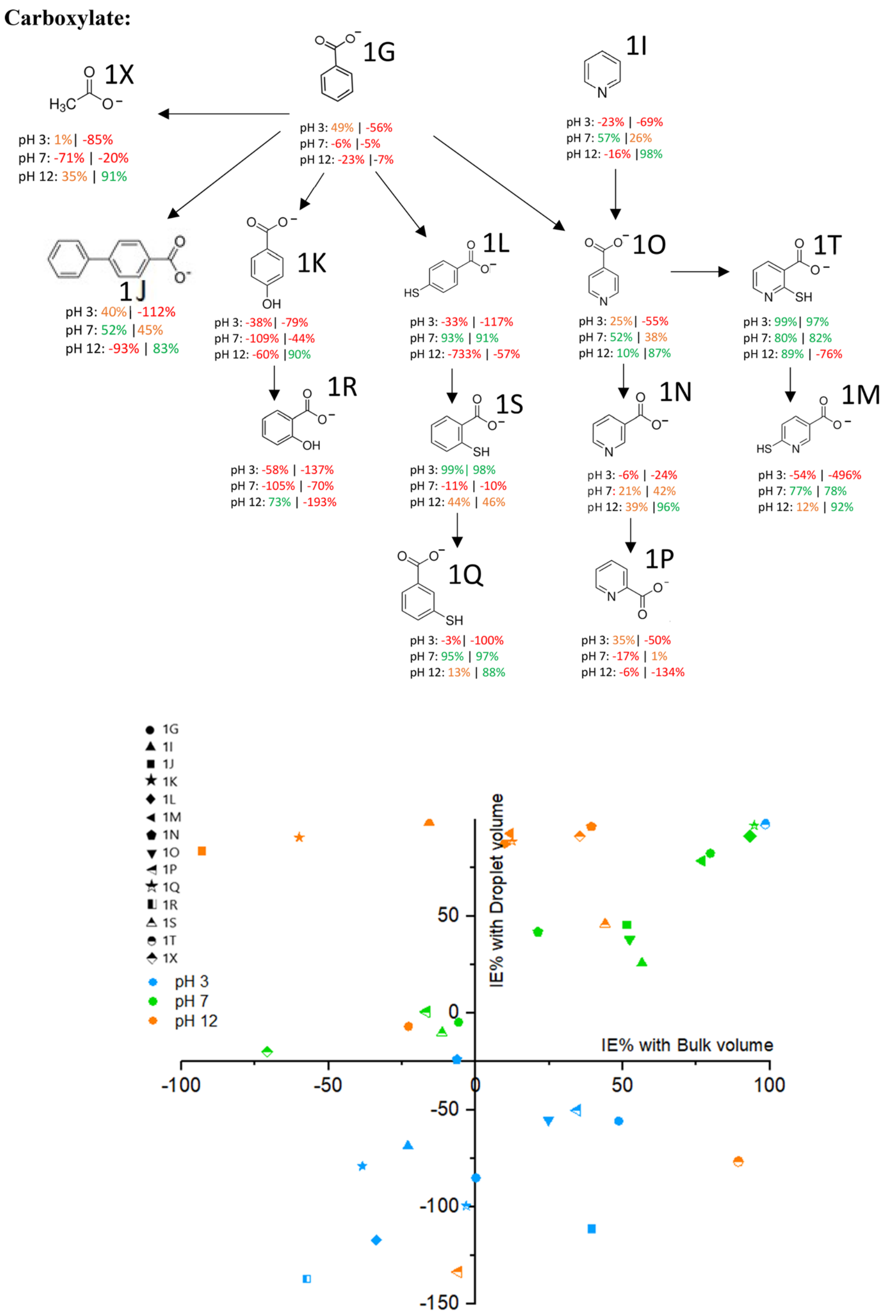

Fig. 8 The inhibition efficiency of inhibitors with a carboxylate group in AA6014 (pH *x*: droplet IE%|bulk IE%).

consist of Fe-rich intermetallic particles.[6,9,43] The $Al_6(Fe, Mn)$ phase is particularly highlighted for causing trenching due to its more noble potential compared to aluminium. The oxygen reduction reaction generates hydroxyl anions, promoting pitting in the matrix near Fe-containing particles. Despite the presence of various intermetallic particles, aluminium alloy AA6*xxx* demonstrates robust corrosion resistance.[44] Mg_2Si acts as an anode in acidic solutions but becomes passive in alkaline conditions, influencing the aluminium matrix differently.[6,45,46] Film-forming organic corrosion inhibitors prove effective in reducing the galvanic activity of intermetallic particles. However, limited literature is available on using organic inhibitors to control intermetallic particle activities in AA6*xxx*.

Conversely, in droplet electrolytes, corrosion is facilitated by abundant oxygen, which readily diffuses over the short distance between the air–electrolyte interface and the metal surface. Evan's droplet theory states that efficient oxygen diffusion occurs at the droplet's edge (cathode), reducing oxygen to generate hydroxide ions (–OH). Simultaneously, the central region (anode) leads to metal loss, oxidizing with hydroxide ions to form rust. This competition for oxygen establishes an oxygen gradient propelling corrosion. The pH gradient within the droplet, induced by the corrosion

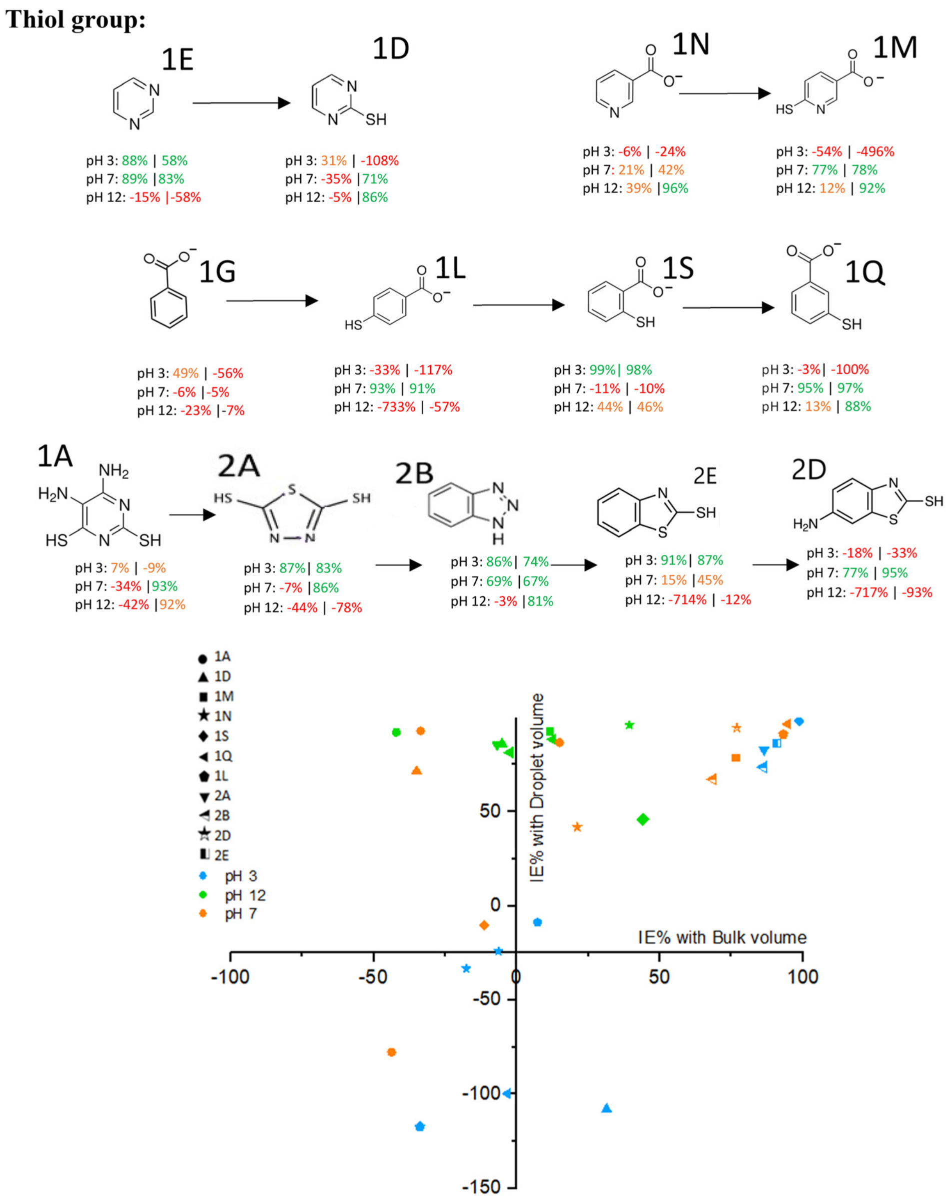

Fig. 9 The inhibition efficiency of inhibitors with a thiol group in AA6014 (pH *x*: droplet IE%|bulk IE%).

reactions, impacts inhibitor performance, with the edge becoming alkaline and the centre acidic. Changes in local conditions over time lead to the development of distinct oxides in different spatial locations within the droplet. These precipitated oxides can hinder charge, oxygen, or ion transfer between the metal and the electrolyte, acting as a barrier to essential processes.

The electrochemical findings presented and discussed in this study underscore the importance of evaluating inhibitory effects in droplet volumes, especially in scenarios involving atmospheric corrosion or other applications with droplets, aerosols, or thin film electrolytes. Given the abundant presence of oxygen, inhibitors may exhibit varying behaviours upon contact with the metal surface. It is evident that the pH of the electrolyte significantly influences inhibitor performance, and this influence differs between bulk and droplet volumes based on the chemical structures of the inhibitors. These results can be attributed to the distinct corrosion mechanisms in droplets compared to the more conventionally understood bulk solution corrosion.

One noteworthy observation is that, under highly alkaline conditions, excluding compounds ineffective in both situations, over 80% of the inhibitors exhibit exceptional performance in droplet volumes (IE% ≥ 75%). In contrast, inhibition efficiency in bulk volumes varies widely, ranging from effective to ineffective, as depicted in Fig. 6. Conversely, under acidic conditions, most compounds appear to be ineffective in droplet volumes compared to bulk volume, with only a few demonstrating excellent performance in both cases.

In bulk volumes, at high pH (>12), the intermetallic Mg_2Si acts as the cathode, and the Al matrix becomes the anode. The amphoteric nature of aluminium oxides under high pH

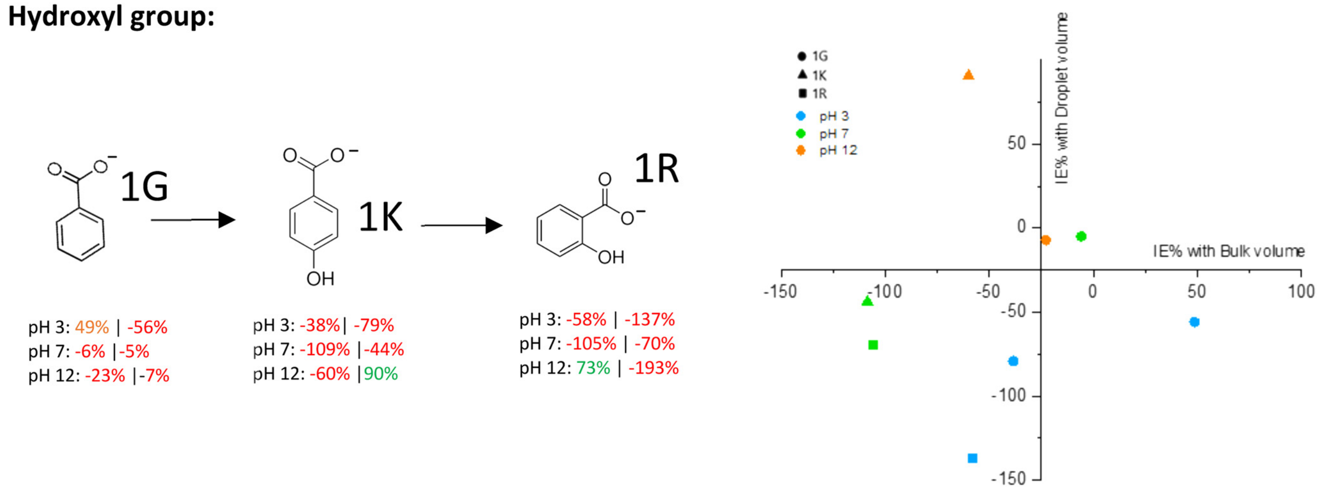

Fig. 10 The inhibition efficiency of inhibitors with a hydroxyl group in AA6014 (pH *x*: droplet IE%|bulk IE%).

conditions could degrade the oxide layers, exposing bulk Al to anodic dissolution.[42] The presence of chloride ions disrupts the stability of the passive layer, potentially reducing the passive range. Conversely, when the solution incorporates an effective inhibitor, it can expand the pH range beyond the typical stability thresholds of aluminium oxide. In systems with chloride ions and inhibitors, a complex interplay of factors makes it challenging to precisely define passivity limits.[32] It's essential to consider that the pH of highly alkaline droplets may change significantly over time due to CO_2 adsorption, which is particularly more pronounced in droplet volumes than in bulk books. This could contribute to the significant difference in results between inhibition efficiency in bulk and droplet volumes. Given these factors, further investigations are imperative to comprehensively study enhanced inhibitor performance under alkaline conditions and reduced inhibitor performance under acidic conditions, particularly within droplet volumes. Such analyses will provide valuable insights into how the corrosion mechanism in droplet environments influences inhibitor efficacy.

Another crucial aspect of this study is examining how chemical functionalities impact the inhibition mechanism in both droplet and bulk volumes. Fig. 9 includes several well-known inhibitor compounds (**2A**, **2B**, **2D**, and **2E**) studied with different alloys. However, compounds **1A** (pH 7: −34%|93%), **2A** (pH 7: −7%|86%), and **2E** (pH 7: 15%|86%) serve as excellent illustrations of how inhibitors that may be ineffective in bulk volumes can prove effective in droplet volumes and *vice versa*.

Fig. 12 illustrates the impact of N and S atoms in compounds on inhibition efficiency. It is evident that, in droplet volume, the inhibition rate rises with an increase in N atoms. However, while optimal inhibition efficiency is achieved with two sulphur atoms, the presence of 3 atoms causes the

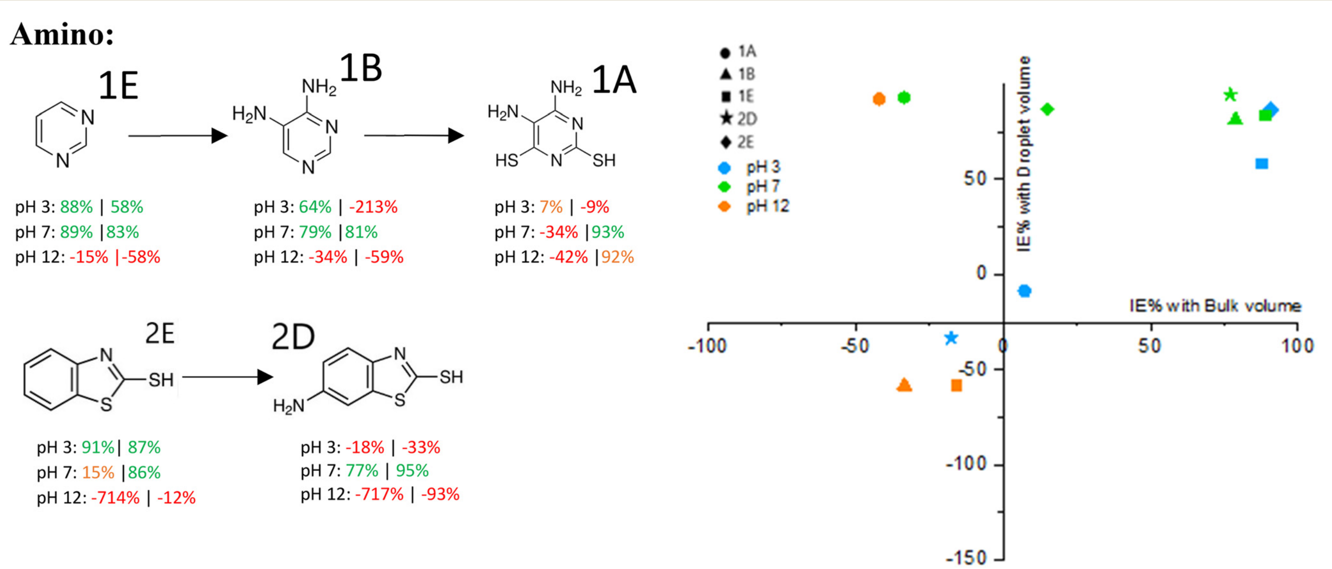

Fig. 11 The inhibition efficiency of inhibitors with amino group in AA6014 (pH *x*: droplet IE%|bulk IE%).

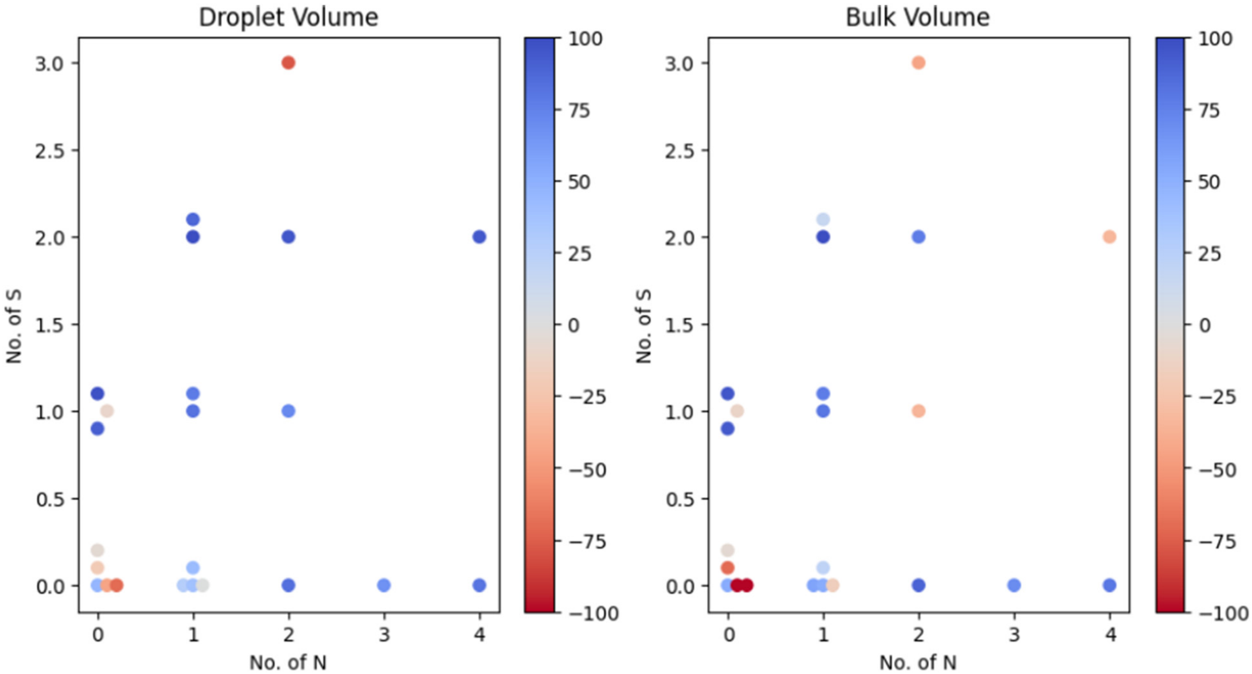

Fig. 12 Sketch map of 23 inhibitor molecules based on their chemical structure with inhibition efficiency incorporated as a colour map.

compound to act as a corrosion accelerator. This may be attributed to multiple functional groups crowding and thereby restricting the formation of a monolayer. This effect is more pronounced in bulk volume, with more N and S inclusions, resulting in a significant drop in inhibition efficiency. Another possibility is that the presence of more than two thiol groups is known to lead to cross-linking, forming disulfides.

Fig. 13 illustrates a schematic map derived from the molecule's polar surface area and molar refractivity. It is noticeable that an optimal inhibition efficiency occurs when the polar surface area falls within the range of 150 to 250.

In droplet volume, higher molar refractivity correlates with improved inhibition than bulk volume, exhibiting irregularities.

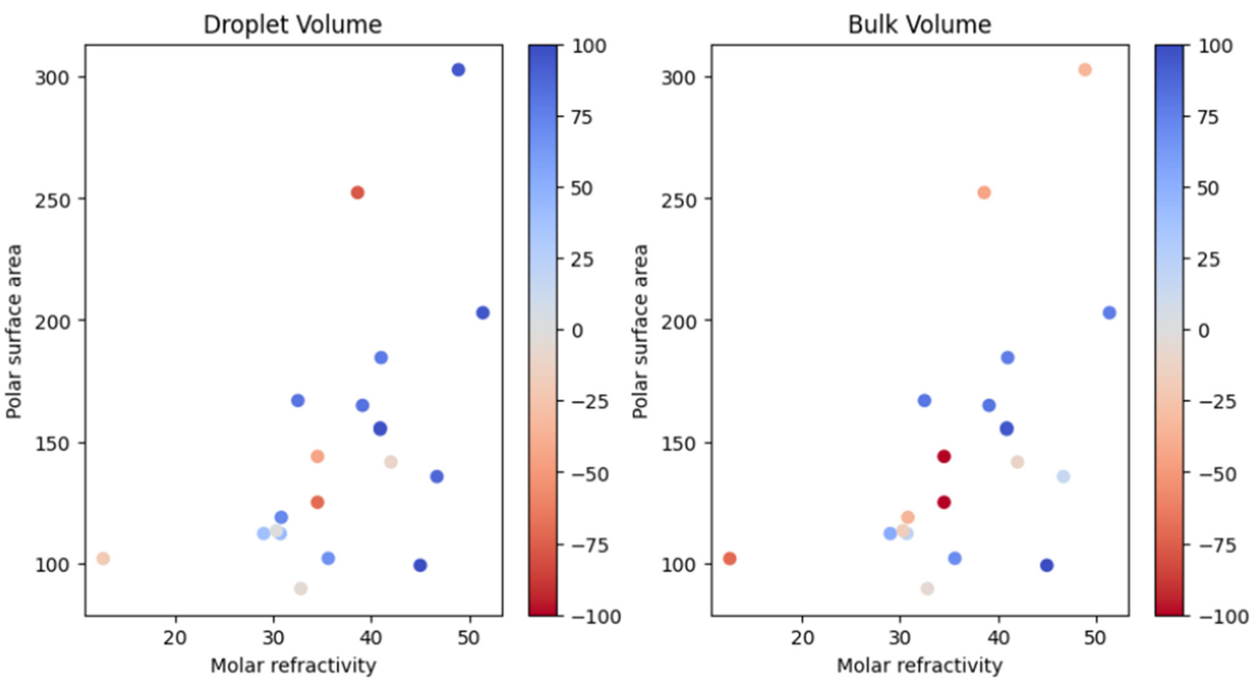

Fig. 13 Sketch map of 23 inhibitor molecules based on their molar refractivity and polar surface area with inhibition efficiency incorporated as a colour map.

Interestingly, a higher polar surface area demonstrates less inhibition in both cases.

It is essential to comprehend how the chemical structure of an inhibitor influences its performance. Therefore, additional studies should be conducted to evaluate this aspect thoroughly.

4. Conclusion

A novel multielectrode electrochemical cell setup was developed to assess inhibitor performance in droplet volumes, addressing the limitations of conventional electrochemical cells designed for bulk volumes. This multielectrode system enables instant attainment of a steady state and concurrent measurement of cathodic and anodic activity, which is crucial for evaluating the performance of multifunctional inhibitors. By eliminating the need for extended time to reach a steady state, tests can be conducted swiftly, facilitating rapid screening of inhibitors to determine their efficacy. A measurement system analysis (MSA) was performed for both droplet and bulk volumes, achieving a variation of less than 20%, thereby qualifying this technique as a viable method for testing with the potential for future enhancements.

A variety of chemically related structures were examined in a 5 wt% NaCl solution to assess their corrosion inhibition capabilities on AA6014. These compounds were tested in droplet volumes of 800 μL and bulk volumes of 80 ml at pH 3, 7, and 12, utilizing a polarization test to determine inhibition efficiency (%). The results indicate that while some inhibitors exhibit close performance between droplet and bulk volumes, others display significant differences.

It was found that most inhibitors were ineffective in droplet volumes, whereas under alkaline conditions, a majority were effective in droplet volume. However, in bulk volume, the performance of the inhibitor ranged from effective to ineffective in equal measure. These data were further analysed to understand the dependency of different functional groups on inhibitor performance. Future studies should aim to expand the range of inhibitors to encompass a broader spectrum of structural and functional variations for a more comprehensive understanding.

Author contributions

Chathumini Samarawickrama: conceptualisation, formal analysis, investigation, writing – original draft preparation. Sebastian Pöhlker: data curation, formal analysis, methodology. Paul White: supervision, writing – review & editing. Patrick Keil: supervision, funding acquisition, conceptualisation, writing – review & editing. Ivan Cole: supervision, funding acquisition, conceptualisation, writing – review & editing.

Conflicts of interest

There are no conflicts to declare.

Acknowledgements

We acknowledge Dr. Milan J Patel (RMIT University) for teaching of programming principles and coding underlying Fig. 11 and 12.

References

1 L. Saberi and M. Amiri, Modeling Atmospheric Corrosion under Dynamic Thin Film Electrolyte, *J. Electrochem. Soc.*, 2021, **168**(8), 081506, DOI: 10.1149/1945-7111/ac1b24.
2 I. S. Cole, Recent progress and required developments in atmospheric corrosion of galvanised steel and zinc, *Materials*, 2017, **10**(11), 1288.
3 Y. Liu, Z. Wang, G. Cao, Y. Cao and Y. Huo, Study on corrosion behavior of zinc exposed in coastal-industrial atmospheric environment, *Mater. Chem. Phys.*, 2017, **198**, 243–249.
4 J. Dong, E. Han and W. Ke, Introduction to atmospheric corrosion research in China, *Sci. Technol. Adv. Mater.*, 2007, **8**(7), 559–565, DOI: 10.1016/j.stam.2007.08.010.
5 I. Cole, N. Azmat, A. Kanta and M. Venkatraman, What really controls the atmospheric corrosion of zinc? Effect of marine aerosols on atmospheric corrosion of zinc, *Int. Mater. Rev.*, 2009, **54**(3), 117–133.
6 M. Jakeria, L. Ward and I. Cole, Long term durability studies on the corrosion inhibition effect of 2-mercaptobenzimidazole (C3H4N2S) on AA6022: mechanism of film formation and influence of IMPs, *Surf. Interfaces*, 2021, **25**, 101164.
7 T. Hausöl, H. W. Höppel and M. Göken, Microstructure and Mechanical Properties of Accumulative Roll Bonded AA6014/AA5754 Aluminium Laminates, *Mater. Sci. Forum*, 2011, **667–669**, 217–222, DOI: 10.4028/www.scientific.net/MSF.667-669.217.
8 K. Alexander, W. Daniel and M. Marion, Influence of a short term heat treatment by conduction and induction on the mechanical properties of AA6014 alloys, *Phys. Procedia*, 2014, **56**, 1410–1418.
9 A. Aballe, M. Bethencourt, F. J. Botana, M. J. Cano and M. Marcos, Inhibition of the corrosion process of alloy AA5083 (Al-Mg) in seawater by cerium cations. An EIS study, *Mater. Corros.*, 2001, **52**(5), 344–350, DOI: 10.1002/1521-4176(200105)52:5<344::AID-MACO344>3.0.CO;2-S.
10 O. F. Hosseinabadi and M. R. Khedmati, A review on ultimate strength of aluminium structural elements and systems for marine applications, *Ocean Eng.*, 2021, **232**, 109153, DOI: 10.1016/j.oceaneng.2021.109153.
11 C. Vargel, Chapter D.3 - Seawater, in *Corrosion of Aluminium*, ed. C. Vargel, Elsevier, Amsterdam, 2004, pp. 335–351.
12 T. G. Harvey, *et al.*, The effect of inhibitor structure on the corrosion of AA2024 and AA7075, *Corros. Sci.*, 2011, **53**(6), 2184–2190, DOI: 10.1016/j.corsci.2011.02.040.
13 N. Van den Steen, Y. Gonzalez-Garcia, J. M. C. Mol, H. Terryn and Y. Van Ingelgem, Predicting the effect of droplet geometry and size distribution on atmospheric corrosion, *Corros. Sci.*, 2022, **202**, 110308, DOI: 10.1016/j.corsci.2022.110308.

14 B. G. Koushik, N. Van den Steen, M. H. Mamme, Y. Van Ingelgem and H. Terryn, Review on modelling of corrosion under droplet electrolyte for predicting atmospheric corrosion rate, *J. Mater. Sci. Technol.*, 2021, **62**, 254–267, DOI: 10.1016/j.jmst.2020.04.061.

15 X. Tang, C. R. Ma, M. E. Orazem, C. You and Y. Li, Local electrochemical characteristics of pure iron under a saline droplet I: Effect of droplet size on electrochemical distribution, *Electrochim. Acta*, 2020, **354**, 136633, DOI: 10.1016/j.electacta.2020.136633.

16 S. R. Street, A. J. M. C. Cook, H. B. Mohammed-Ali, T. Rayment and A. J. Davenport, The Effect of Deposition Conditions on Atmospheric Pitting Corrosion Location Under Evans Droplets on Type 304L Stainless Steel, *Corrosion*, 2018, **74**(5), 520–529, DOI: 10.5006/2614.

17 T. H. Muster, *et al.*, The atmospheric corrosion of zinc: The effects of salt concentration, droplet size and droplet shape, *Electrochim. Acta*, 2011, **56**(4), 1866–1873, DOI: 10.1016/j.electacta.2010.09.099.

18 I. S. Cole, N. S. Azmat, A. Kanta and M. Venkatraman, What really controls the atmospheric corrosion of zinc Effect of marine aerosols on atmospheric corrosion of zinc?, *Int. Mater. Rev.*, 2009, **54**(3), 117–133, DOI: 10.1179/174328009X411145.

19 I. Cole, T. Muster, D. Lau, N. Wright and N. S. Azmat, Products formed during the interaction of seawater droplets with zinc surfaces: II. Results from short exposures, *J. Electrochem. Soc.*, 2010, **157**(6), C213.

20 M. S. Venkatraman, I. S. Cole, D. R. Gunasegaram and B. Emmanuel, Modeling Corrosion of a Metal under an Aerosol Droplet, *Mater. Sci. Forum*, 2010, **654–656**, 1650–1653, DOI: 10.4028/www.scientific.net/MSF.654-656.1650.

21 N. S. Azmat, K. D. Ralston, B. C. Muddle and I. S. Cole, Corrosion of Zn under acidified marine droplets, *Corros. Sci.*, 2011, **53**(4), 1604–1615, DOI: 10.1016/j.corsci.2011.01.044.

22 N. S. Azmat, K. D. Ralston, B. C. Muddle and I. S. Cole, Corrosion of Zn under fine size aerosols and droplets using inkjet printer deposition and optical profilometry quantification, *Corros. Sci.*, 2011, **53**(11), 3534–3541, DOI: 10.1016/j.corsci.2011.06.028.

23 P. C. King, I. S. Cole, P. A. Corrigan, A. E. Hughes, T. H. Muster and S. Thomas, FIB/SEM study of AA2024 corrosion under a seawater drop, part II, *Corros. Sci.*, 2012, **55**, 116–125, DOI: 10.1016/j.corsci.2011.10.012.

24 S. C. Morton and G. S. Frankel, Atmospheric pitting corrosion of AA7075-T6 under evaporating droplets with and without inhibitors, *Mater. Corros.*, 2014, **65**(4), 351–361, DOI: 10.1002/maco.201307363.

25 S. P. Knight, A. D. Sudholz, A. Butler, S. Palanisamy, M. S. Dargusch and A. R. Trueman, The effect of droplet size on the localized corrosion of high-strength aluminum alloys: Effect of droplet size on localized corrosion of Al alloys, *Mater. Corros.*, 2016, **67**(12), 1294–1307, DOI: 10.1002/maco.201609045.

26 M. Liu, Q. Yin, Y. Liu, C. Pan, C. Wang and Z. Wang, Secondary spreading of acidified aerosols on the surface of Zn, *J. Mater. Res. Technol.*, 2020, **9**(3), 2635–2644, DOI: 10.1016/j.jmrt.2019.12.091.

27 X. Tang, C. R. Ma, M. E. Orazem, C. You and Y. Li, Local electrochemical characteristics of pure iron under a saline droplet II: Local corrosion kinetics, *Electrochim. Acta*, 2020, **354**, 136631, DOI: 10.1016/j.electacta.2020.136631.

28 C. Chen and F. Mansfeld, Potential distribution in the evans drop experiment, *Corros. Sci.*, 1997, **39**(2), 409–413, DOI: 10.1016/S0010-938X(97)83355-0.

29 F. Lequien, *et al.*, Corrosion influence on the evaporation of sessile droplet, *Colloids Surf., A*, 2018, **546**, 59–66, DOI: 10.1016/j.colsurfa.2018.02.047.

30 P. C. King, I. S. Cole, P. A. Corrigan, A. E. Hughes and T. H. Muster, FIB/SEM study of AA2024 corrosion under a seawater drop: Part I, *Corros. Sci.*, 2011, **53**(3), 1086–1096, DOI: 10.1016/j.corsci.2010.12.004.

31 M. S. Venkatraman, I. S. Cole, D. R. Gunasegaram and B. Emmanuel, Modeling corrosion of a metal under an aerosol droplet, in *Materials Science Forum*, Trans Tech Publ, 2010, vol. 654, pp. 1650–1653.

32 S. García, *et al.*, The influence of pH on corrosion inhibitor selection for 2024-T3 aluminium alloy assessed by high-throughput multielectrode and potentiodynamic testing, *Electrochim. Acta*, 2010, **55**(7), 2457–2465.

33 S. R. Taylor and B. D. Chambers, *Proceedings of the 4th International Symposium on Aluminium Surface Science and Technology*, Beaune, France, 2006.

34 T. H. Muster, *et al.*, A rapid screening multi-electrode method for the evaluation of corrosion inhibitors, *Electrochim. Acta*, 2009, **54**(12), 3402–3411, DOI: 10.1016/j.electacta.2008.12.051.

35 S. J. Garcia, *et al.*, Validation of a fast scanning technique for corrosion inhibitor selection: influence of cross-contamination on AA2024-T3: Validation of multielectrode for corrosion inhibitor selection, *Surf. Interface Anal.*, 2010, **42**(4), 205–210, DOI: 10.1002/sia.3150.

36 S. Taylor and M. Kendig, Rapid discovery of corrosion inhibitors and synergistic combinations using high-throughput screening methods, *Corrosion*, 2005, **61**(05), 480–489, DOI: 10.5006/1.3280648.

37 C. Samarawickrama, X.-B. Chen, R. J. Toh, P. Keil and I. Cole, Comparison betwen the performance of a corrosion inhibitor by droplet and bulk volume for AA6014, in *Corrosion and Prevention*, Australasian Corrosion Association, Newcastle, Australia, 2021.

38 M. Meeusen, P. Visser, L. Fernández Macía, A. Hubin, H. Terryn and J. M. C. Mol, The use of odd random phase electrochemical impedance spectroscopy to study lithium-based corrosion inhibition by active protective coatings, *Electrochim. Acta*, 2018, **278**, 363–373, DOI: 10.1016/j.electacta.2018.05.036.

39 B. E. Risteen, E. Schindelholz and R. G. Kelly, Marine Aerosol Drop Size Effects on the Corrosion Behavior of Plain Carbon Steel, *ECS Trans.*, 2014, **58**(29), 1–12, DOI: 10.1149/05829.0001ecst.

40 M. Pourbaix, *Atlas of electrochemical equilibria in aqueous solutions*, NACE, 1966.

41 K. Nisancioglu, *9 – Corrosion and protection of aluminum alloys in seawater*, 2007.
42 M. R. Jakeria, R. J. Toh, X.-B. Chen and I. S. Cole, Evolution and stability of 2-mercaptobenzimidazole inhibitor film upon Al alloy 6061, *J. Appl. Electrochem.*, 2022, **52**(6), 1021–1044, DOI: **10.1007/s10800-022-01687-w**.
43 J. F. Li, B. Maier and G. S. Frankel, Corrosion of an Al-Mg-Si alloy under MgCl2 solution droplets, *Corros. Sci.*, 2011, **53**(6), 2142–2151, DOI: **10.1016/j.corsci.2011.02.035**.
44 S. K. Kairy and N. Birbilis, Clarifying the role of Mg2Si and Si in localized corrosion of aluminum alloys by quasi in situ transmission electron microscopy, *Corrosion*, 2020, **76**(5), 464–475.
45 M. H. Larsen, J. C. Walmsley, O. Lunder and K. Nisancioglu, Effect of excess silicon and small copper content on intergranular corrosion of 6000-series aluminum alloys, *J. Electrochem. Soc.*, 2009, **157**(2), C61.
46 Y. Zhang, B. Milkereit, O. Kessler, C. Schick and P. Rometsch, Development of continuous cooling precipitation diagrams for aluminium alloys AA7150 and AA7020, *J. Alloys Compd.*, 2014, **584**, 581–589.